LANDMARK-BASED ELASTIC MATCHING OF TOMOGRAPHIC IMAGES

K. Rohr[1], *H.S. Stiehl*[1], *R. Sprengel*[1], *W. Beil*[1], *T.M. Buzug*[2], *J. Weese*[2], *and M.H. Kuhn*[2]

[1] Universität Hamburg, Fachbereich Informatik, Arbeitsbereich Kognitive Systeme, Vogt-Kölln-Str. 30, D-22527 Hamburg, Germany

[2] Philips Research, Technical Systems Hamburg, Röntgenstr. 24-26, D-22335 Hamburg

ABSTRACT

We describe a novel approach for elastic matching of tomographic images of the human brain. The approach is based on a set of corresponding anatomical point landmarks and uses approximating thin-plate splines. Previous work on this topic has concentrated on using interpolation schemes which means that corresponding landmarks are exactly matched to each other. Consequently, the underlying assumption is that the landmark positions are known exactly. However, in real applications the localization of landmarks is always prone to error. Therefore, to cope with these errors, we have investigated the application of an approximation scheme which is based on a minimizing functional. This approach renders possible to individually weight the landmarks according to their localization uncertainty. Our approach has been applied to 2D as well as 3D tomographic data.

1. INTRODUCTION

In neurosurgery and radiotherapy planning it is important to either register images from different modalities, e.g. CT (X-ray Computed Tomography) and MR (Magnetic Resonance) images, or to match images to atlas representations. If only *rigid* transformations were applied, then the accuracy of the resulting match often is not satisfactory w.r.t. clinical requirements. In general, *nonrigid* or *elastic* transformations are required to cope with the variations between the data sets.

This contribution is concerned with elastic matching of medical image data based on a set of corresponding anatomical point landmarks. Previous work on this topic has concentrated on i) selecting the corresponding landmarks manually and on ii) using an interpolating transformation model (Bookstein [2], Evans et al. [6], and Mardia and Little [13]). The basic approach draws upon thin-plate splines and is computationally efficient, robust, and general w.r.t. different types of images and atlases. Also, the approach is well-suited for user-interaction which is important in clinical scenaria. However, an interpolation scheme forces the corresponding landmarks to exactly match each other. The underlying assumption is that the landmark positions are known exactly. In real applications, however, the localization of landmarks is always prone to error. This is true for interactive as well as for automatic landmark localization.

Therefore, to take into account these localization errors, we have investigated the application of an approximation scheme where the corresponding thin-plate splines result from regularization theory. Generally, such an approach yields a more accurate and robust registration result. In particular, outliers do not disturb the registration result as much as is the case with an interpolation scheme. Also, it is possible to individually weight the landmarks according to their localization uncertainty. We have applied this approach to elastic matching of tomographic images of the human brain.

We also report on investigations into semi-automatic extraction of anatomical point landmarks using 3D differential operators. Algorithms for this task are important since manual selection of landmarks is time-consuming and often lacks accuracy.

2. CLINICAL APPLICATIONS FOR ELASTIC MATCHING

2.1. Image-atlas matching

One possible application for elastic registration is trajectory planning for neurosurgical intervention. Pain treatment as well as epilepsy treatment sometimes require to localize a functionally important region not visible in the available image data. There are instructions available in the literature how to construct the position of such a region given landmarks which can be identified in CT or MR images. Hence, it is useful to superimpose an atlas with a medical image as already proposed by Talairach. Due to the individual variability of anatomical structures, rigid registration is generally not sufficient and elastic matching should be applied.

2.2. CT-MR matching

Another application is the registration of CT and MR images for the purpose of radiotherapy planning. Additionally, a template atlas can be superimposed on the MR image to indicate, for example, organs at risk. This superposition result is then overlayed on the CT image prior to dose calculation and isodose visualization on the MR image. It is questionable whether rigid registration is suitable for this purpose since MR images are geometrically distorted. On the one hand, scanner-induced distortions have to be coped with which are caused by, e.g., inhomogeneities of the main magnetic field, imperfect slice or volume selection pulses, nonlinearities of the magnetic field gradients, and eddy currents [14]. These distortions can be reduced by suitable calibration steps: The inhomogeneities of the main magnetic field are minimized by passive and active shimming whereas, e.g., the gradient nonlinearities cannot be completely shimmed. Thus, depending on the scanner protocol, the sum of all remaining distortions leads to a residual error of a few millimeters (for a spherical field of view of 25 cm). On the other hand, there are geometrical distortions in MR images that are induced by the patient and cannot be removed by calibration. Parameters such as susceptibility variations, chemical shift of non-water protons and flow-induced distortions for vessels are very important. While the susceptibility difference of tissue and bone is negligible, the susceptibility difference between tissue and air is approximately 10^{-5}. This can result in a field variation of up to 10 ppm and geometrical distortions of more than 5 mm [12],[5] which is most important for the nasal and aural regions. Consequently, due to the scanner- as well as the patient-induced distortions of the MR image, CT and MR images in general cannot be satisfactorily registered using rigid transformations.

3. THIN-PLATE SPLINE APPROXIMATION BASED ON A MINIMIZING FUNCTIONAL

The orginal thin-plate spline interpolation approach introduced by Bookstein [2] (see also [1]) can be extended in such a way that we can take into account landmark localization errors. We achieve this by combining a quadratic approximation criterion with the original smoothness functional:

$$J_\lambda(\mathbf{u}) = \frac{1}{n}\sum_{i=1}^{n} |\mathbf{q}_i - \mathbf{u}(\mathbf{p}_i)|^2 + \lambda J_m^d(\mathbf{u}), \qquad (1)$$

where n is the number of landmarks, d the dimension of the image, and m the order of derivatives in the smoothness functional (see Wahba [20] for a theoretical study of such functionals). The first term (data term) measures the distances between the transformed source landmarks $\mathbf{p}_i$ and the target landmarks $\mathbf{q}_i$. The second term measures the smoothness of the resulting transformation. Hence, the minimization of (1) yields a transformation $\mathbf{u}$, which i) approximates the distance of the source landmarks to the target landmarks and ii) is sufficiently smooth. The relative weight between the approximation behavior and the smoothness of the transformation is determined by the regularization parameter $\lambda > 0$. In the limit of $\lambda \to 0$ we obtain an interpolating transformation, whereas in the limit of $\lambda \to \infty$ we get a global polynomial of order up to $m-1$.

The solution to (1) can be stated analytically as the weighted sum of polynomials ϕ_j and certain radial basis functions U_i using the coefficient vectors $\mathbf{a}$ and $\mathbf{w}$. The computational scheme to compute $\mathbf{a}$ and $\mathbf{w}$ then reads as

$$\begin{aligned} (\mathbf{K} + n\lambda\mathbf{I})\mathbf{w} + \mathbf{P}\mathbf{a} &= \mathbf{v} \\ \mathbf{P}^T\mathbf{w} &= 0, \end{aligned} \qquad (2)$$

where $K_{ij} = U_i(\mathbf{p}_j)$, $P_{ij} = \phi_j(\mathbf{p}_i)$, and $\mathbf{v}$ represents one component of the coordinates of the $\mathbf{q}_i$. The interesting fact is that this scheme is nearly the same as in the case of interpolation. We only have to add $n\lambda$ in the diagonal of the matrix $\mathbf{K}$.

Fig. 1 shows an example of the thin-plate spline approximation scheme in 2D ($m = 2$) for different values of λ. The small black points and big grey points mark the positions of the source and target landmarks, respectively. The top-left part of Fig. 1 shows the regular grid. The top-right part shows the result for $\lambda = 0$, which is equivalent to the interpolation scheme. At some locations the grid is heavily distorted, especially around the two close landmarks in the bottom-left part of this grid. The two bottom grids visualize results for $\lambda = 0.001$ (bottom-left) and $\lambda = 0.1$ (bottom-right), where the latter one nearly yields a pure affine transformation.

A generalization of the approximation scheme can be attained, if information about the accuracy of the landmarks is available. Then, we can weight each single data term in (1) by the variance σ_i^2. If, for example, the variance is high, i.e. landmark localization is uncertain, then the influence on the overall approximation error is weighted low. With this generalization our functional reads

$$J_\lambda(\mathbf{u}) = \frac{1}{n}\sum_{i=1}^{n} \frac{|\mathbf{q}_i - \mathbf{u}(\mathbf{p}_i)|^2}{\sigma_i^2} + \lambda J_m^d(\mathbf{u}), \qquad (3)$$

and we have to solve the following system of equations:

$$\begin{aligned} (\mathbf{K} + n\lambda\mathbf{W}^{-1})\mathbf{w} + \mathbf{P}\mathbf{a} &= \mathbf{v} \\ \mathbf{P}^T\mathbf{w} &= 0, \end{aligned} \qquad (4)$$

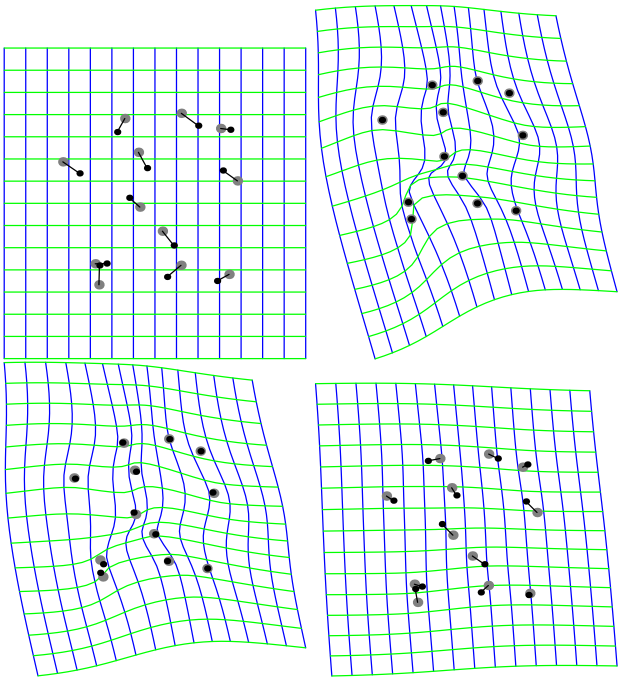

Figure 1: Thin-plate spline approximation (input data, $\lambda = 0, 0.001$, and 0.1).

where $\mathbf{W} = \mathrm{diag}\{1/\sigma_1^2, \ldots, 1/\sigma_n^2\}$ (see also [16], [18]). Note, that this approach can be applied to images of arbitrary dimension, i.e. in particular to 2D as well as 3D images.

For a different approach to relax the interpolation conditions see Bookstein [4]. However, this approach has been not been related to a minimizing functional, but merely combines different metrics. Additionally, this approach is only described for 2D datasets ($d = m = 2$) and has only been applied to 2D synthetic data ('simulated PET images').

4. EXPERIMENTAL RESULTS

4.1. 2D Data

Within the scenario of CT-MR registration as discussed above we here consider the application of correcting patient-induced susceptibility distortions of MR images. To this end we have acquired two sagittal MR images of a healthy human volunteer brain with typical susceptibility distortions. In our experiment we used a high-gradient MR image as "ground truth" (instead of clinically common CT images) to avoid exposure of the volunteer to radiation. Both turbo-spin echo images have consecutively been acquired on a modified Philips $1.5T$ MR scanner with a slice thickness of $4mm$ without repositioning. Therefore, we are sure that we actually have identical slicing in space. Using a gradient of $1mT/m$ and $6mT/m$ for the first and second image then leads to a shift of ca. $7.5...10mm$ and ca. $1.3...1.7mm$, respectively.

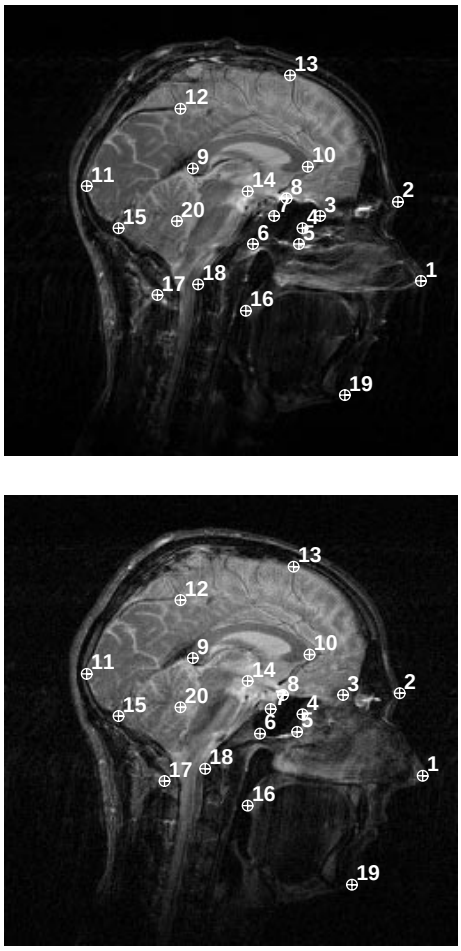

Figure 2: Original MR images with landmarks: First (top) and second (bottom) image.

Within each of the two images we have manually selected 20 point landmarks. To simulate outliers, one of the landmarks in the second image (No. 3) has been shifted about 15 pixels away from its true position for demonstration purposes (see Fig. 2). Note, however, that manual localization of landmarks actually can be prone to relatively large errors. Fig. 3 shows the results of the interpolating vs. the approximating thin-plate spline approach. Each result represents the transformed first image. It can be seen that the interpolation scheme yields a rather unrealistic deformation since it forces all landmark pairs, including the pair with the simulated outlier, to exactly match each other. Using our approximation scheme instead yields a more accurate registration result.

4.2. 3D Data

We have applied our registration scheme also to 3D data. In our experiment, we have simulated nonlinear

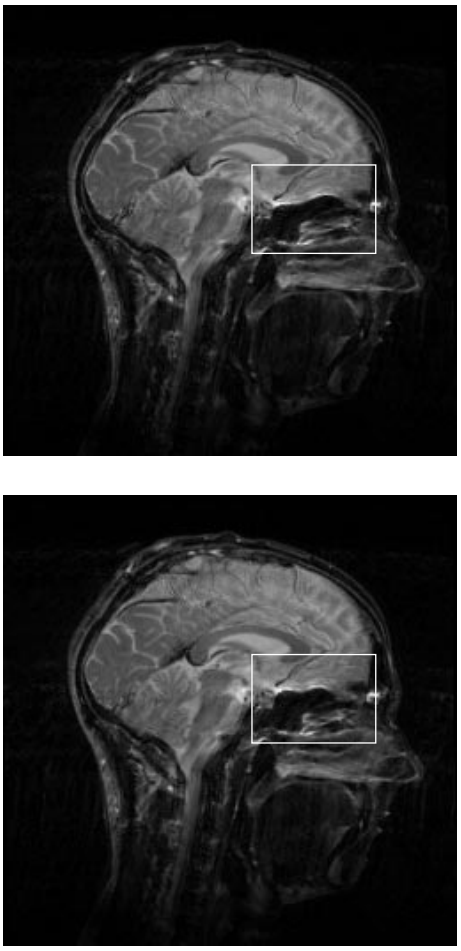

Figure 3: Registration results: Interpolation (top) and approximation (bottom).

deformations of the digital SAMMIE atlas [10]. One slice of this 3D human brain atlas is shown in Fig. 4 on the left. Different anatomical structures are labeled with different gray values. The deformed atlas with overlayed contours from the original atlas is shown on the right. It can be seen that the deformations are relatively large.

To register the deformed atlas with the original atlas, we have manually specified 34 homologous landmarks and have added Gaussian noise to the landmark positions such as to simulate typical localization errors (see also [17]). A different noise level has been chosen for each landmark, with standard deviations σ_i in the range between 0.5 and 3.5 voxels. For our experiment this resulted in displacements between 0.5 and 7 voxels which are to be expected for manual landmark localization.

Fig. 5 on the left shows the result of applying the approximating thin-plate spline approach with $\lambda = 0.5$ to the 3D atlas data. For the weights in (3) we have used values in accordance to the simulated

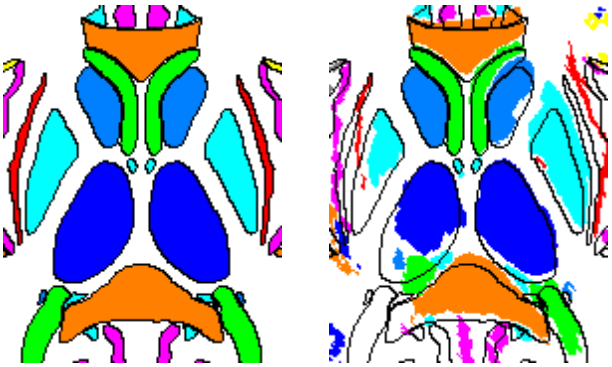

Figure 4: Original and deformed 3D human brain atlas.

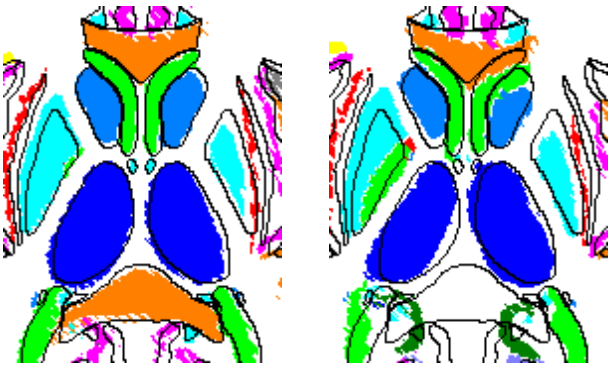

Figure 5: Thin-plate spline approximation with individually weighted landmarks: $\lambda = 0.5$ (left), $\lambda = \infty$ (affine approximation) (right).

noise levels. We have also computed the registration result for a pure affine transformation (limiting case of $\lambda = \infty$ of approximating thin-plate splines; see Fig. 5 on the right) while using the same weights as before. As can be seen, the registration result with approximating thin-plate splines is significantly better in comparison to a pure affine transformation, particularly in the lower part of the image.

5. SEMI-AUTOMATIC LOCALIZATION OF ANATOMICAL POINT LANDMARKS

One main problem with point landmarks is their reliable and accurate extraction from 3D images. Therefore, 3D point landmarks have usually been selected manually (e.g., Evans et al. [6], Hill et al. [9]; but see also Thirion [19]). In the following, we describe our investigations into semi-automatic localization of 3D anatomical point landmarks. Semi-automatic means that either a region-of-interest (ROI) or an approximate position of a specific landmark (or both) is given by the user. Then, an algorithm has to provide a refined position of the landmark. Alternatively, land-

mark candidates for a large ROI or even for the whole data set may be provided automatically from which the final set of landmarks is selected manually. Such a semi-automatic approach has the advantage that a user has the possibility to control the results ("keep-the-user-in-the-loop").

Within a ROI we apply specific 3D differential operators such as to exploit the knowledge about a landmark as far as possible, in particular it's geometric structure. To localize curvature extrema we use an operator which estimates Gaussian curvature, i.e. the product of the two principal curvatures $K = \lambda_1 \lambda_2$, multiplied with the fourth power of the gradient magnitude $|\nabla g|$. Fig. 6 shows a result of this operator for the right frontal horn in a 3D MR image in sagittal, axial, and coronal view. It can be seen that we obtain a strong operator response at the tip of the frontal horn.

We also investigate 3D differential operators which are extensions of existing 2D 'corner detectors'. For an analytic study of such 2D operators see Rohr [15]. These operators have the advantage that only low order partial derivatives of the image function are necessary (either first or first and second order). Therefore, these operators are computationally efficient. Recently, we have compared the 2D operators w.r.t. their detection capabilities on a larger number of 2D tomographic images of the human brain (see Hartkens et al. [8]). In Fig. 7 we show, as an example, the application of the 2D operator of Förstner [7] vs. a 3D extension of it: $det\underline{C}_g / trace\underline{C}_g \rightarrow max$, where $\underline{C}_g = \overline{\nabla g \, (\nabla g)^T}$ and ∇g denotes the image gradient in 2D and 3D, respectively. Note, that in the 2D case many well detected landmarks agree with the manually selected landmarks in Bookstein [3]. Note also, that the 3D operator actually takes into account the 3D structure of the landmarks and therefore in a single slice of a 3D image only a few of the 3D point landmarks are visible, i.e., other landmarks according to [3] have been detected in different slices.

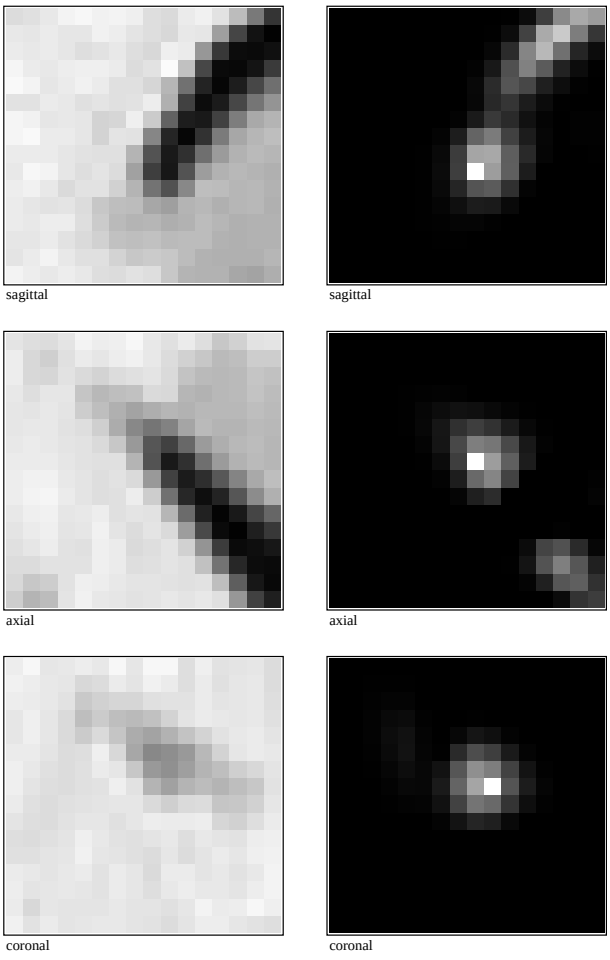

Figure 6: Right frontal horn in a 3D MR data set (left) and result of computing the 3D Gaussian curvature (right) in sagittal, axial, and coronal view

Acknowledgement

Support of Philips Research Hamburg, project IMAGINE (IMage- and Atlas-Guided Interventions in NEurosurgery), and of the EU, project EASI (contract HC1012) is gratefully acknowledged. We would like to thank K. Jungnickel (formerly with Philips Research Hamburg) for providing us with the MR images showing the susceptibility distortions. We are also indebted to F.J. Schuier and T. Wittkopp for making available the SAMMIE atlas developed within the EU project SAMMIE (contract A2032).

6. REFERENCES

[1] L. Binder, K. Rohr, R. Sprengel, and H. Stiehl. Bildregistrierung mit interpolierenden 'Thin-Plate Splines' und Bezüge zur linearen Elastizitätstheorie. In Jähne et al. [11], pages 281–288.

[2] F. Bookstein. Principal warps: Thin-plate splines and the decomposition of deformations. *IEEE Trans. on Pattern Anal. and Machine Intell.*, 11(6):567–585, 1989.

[3] F. Bookstein. Thin-plate splines and the atlas problem for biomedical images. In A. Colchester and D. Hawkes, editors, *12th Internat. Conf. Information Processing in Medical Imaging*, volume 511 of *Lecture Notes in Computer Science*, pages 326–342, Wye/UK, 1991. Springer Berlin Heidelberg.

[4] F. L. Bookstein. Four metrics for image variation. In D. Ortendahl and J. Llacer, editors, 11^{th} *International Conference on Information*

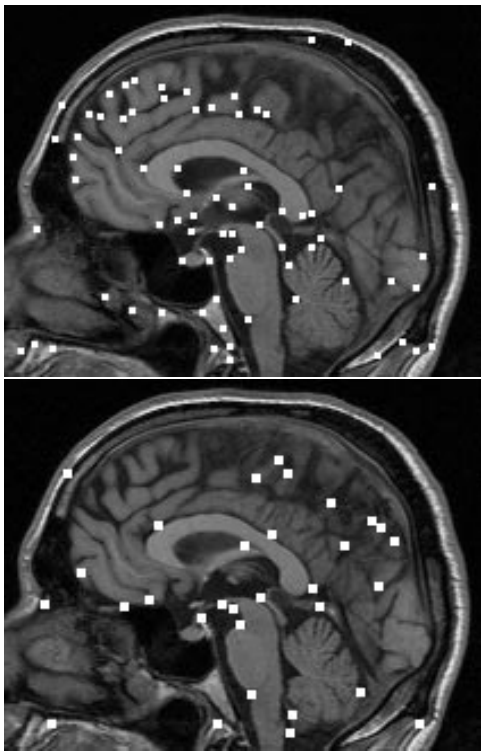

Figure 7: Landmark candidates: Application of a 2D 'corner' detector (top) vs. a 3D extension (bottom) on a 2D and 3D MR image, respectively.

Processing in Medical Imaging (IPMI-89), volume 363 of *Progress in Clinical and Biological Research*, pages 227–240. Wiley-Liss, Inc., New York, 1991.

[5] H. Chang and J. Fitzpatrick. A technique for accurate magnetic resonance imaging in the presence of field inhomogeneities. *IEEE Trans. Med. Imaging*, 11:319, 1992.

[6] A. Evans, W. Dai, L. Collins, P. Neelin, and S. Marrett. Warping of a computerized 3-d atlas to match brain image volumes for quantitative neuroanatomical and functional analysis. In M. Loew, editor, *Medical Imaging V: Image Processing*, volume 1445 of *Proc. SPIE*, pages 236–246, San Jose, CA, 1991.

[7] W. Förstner. A feature based correspondence algorithm for image matching. *Intern. Arch. of Photogrammetry and Remote Sensing*, 26-3/3:150–166, 1986.

[8] T. Hartkens, K. Rohr, and H. Stiehl. Evaluierung von Differentialoperatoren zur Detektion charakteristischer Punkte in tomographischen Bildern. In Jähne et al. [11], pages 637–644.

[9] D. Hill, D. Hawkes, J. Crossman, M. Gleeson, T. Cox, E. Bracey, A. Strong, and P. Graves. Registration of MR and CT images for skull base surgery using point-like anatomical features. *The British J. of Radiology*, 64(767):1030–1035, 1991.

[10] U. Hübner, F. J. Schuier, and J. A. Newell. SAMMIE A203: software applied to multimodal images and education. *Computer Methods and Programs in Biomedicine*, 45:149–152, 1994.

[11] B. Jähne, P. Geißler, H. Haußecker, and F. Hering, editors. *18. DAGM-Symposium Mustererkennung*, Informatik aktuell. Springer Berlin Heidelberg, 1996.

[12] K. Lüdeke, P. Röschmann, and R. Tischler. Susceptibility artifacts in nmr imaging. *MRI*, 3:329, 1985.

[13] K. Mardia and J. Little. Image warping using derivative information. In F. Bookstein, J. Duncan, N. Lange, and D. Wilson, editors, *Mathematical Methods in Medical Imaging III*, volume 2299 of *Proc. SPIE*, pages 16–31, San Diego, CA, 25-26 July 1994.

[14] J. Michiels, H. Bosmans, P. Pelgrims, D. Vandermeulen, J. Gybels, G. Marchal, and P. Suetens. On the problem of geometric distortion in magnetic resonance images for stereotactic neurosurgery. *Mag. Res. Imag.*, 12:749, 1994.

[15] K. Rohr. Localization properties of direct corner detectors. *J. of Mathematical Imaging and Vision*, 4(2):139–150, 1994.

[16] K. Rohr, H. S. Stiehl, R. Sprengel, W. Beil, T. M. Buzug, J. Weese, and M. H. Kuhn. Point-based elastic registration of medical image data using approximating thin-plate splines. In K. Höhne and R. Kikinis, editors, *4th Internat. Conf. Visualization in Biomedical Computing (VBC'96)*, volume 1131 of *Lecture Notes in Computer Science*, pages 297–306. Springer Berlin Heidelberg, 1996.

[17] R. Sprengel, K. Rohr, and H. S. Stiehl. Properties and extensions of the thin-plate spline approach for image registration. Techn. Report FBI-HH-M-267/96, FB Informatik, Universität Hamburg, Dec. 1996.

[18] R. Sprengel, K. Rohr, and H. S. Stiehl. Thin-plate spline approximation for image registration. In *18th Internat. Conf. of the IEEE Engineering in Medicine and Biology Society (EMBS'96)*, Amsterdam, The Netherlands, 1996.

[19] J.-P. Thirion. Extremal points: definition and application to 3d image registration. In *Proc. IEEE Conf. on Computer Vision and Pattern Recognition*, pages 587–592, Seattle/Washington, USA, 1994.

[20] G. Wahba. *Spline Models for Observational Data*. Society for Industrial and Applied Mathematics, Philadelphia, Pennsylvania, 1990.